Nucleation and growth of insulin fibrils in bulk solution and at hydrophobic polystyrene surfaces

M.I. Smith and J.S. Sharp[1,2]
School of Physics and Astronomy and Nottingham Nanotechnology and Nanoscience Centre,
The University of Nottingham, Nottingham, NG7 2RD, UK

C.J. Roberts
Laboratory of Biophysics and Surface Analysis, School of Pharmacy and Nottingham Nanotechnology and Nanoscience Centre, The University of Nottingham, Nottingham, NG7 2RD, UK

Abstract

A new technique was developed for studying the nucleation and growth of fibrillar protein aggregates. Fourier transform infra-red (FTIR) and attenuated total reflection (ATR) spectroscopy were used to measure changes in the intermolecular β-sheet content of bovine pancreatic insulin (BPI) in bulk solution and on model Polystyrene (PS) surfaces at pH 1. The kinetics of β-sheet formation were shown to evolve in two stages. Combined FTIR, dynamic light scattering, atomic force microscopy and ThT fluorescence measurements confirmed that the first stage in the kinetics was related to the formation of non-fibrillar aggregates that have a radius of ~ 13*nm*. The second stage was found to be associated with the growth of insulin fibrils. The β-sheet kinetics in this second stage were used to determine the nucleation and growth rates of fibrils over a range of temperatures between 60^oC and 80^oC. The nucleation and growth rates were shown to display Arrhenius kinetics and the associated energy barriers were extracted for fibrils formed in bulk solution and at PS surfaces. These experiments showed that fibrils are nucleated more quickly in the presence of hydrophobic PS surfaces but that the corresponding fibril growth rates decrease. These observations are interpreted in terms of the differences in the attempt frequencies and energy barriers associated with the nucleation and growth of fibrils. They are also discussed in the context of differences in protein concentration, mobility, conformational and colloidal stability that exist between insulin molecules in bulk solution and those that are localised at hydrophobic PS interfaces.

[1]Corresponding author:james.sharp@nottingham.ac.uk
[2]web site: www.nottingham.ac.uk/physics/research/nano

Keywords: Insulin, Amyloid fibrils, Surfaces and Interfaces, Nanotoxicology, Energy Barriers, FTIR spectroscopy, nucleation, growth

INTRODUCTION

The effects of surfaces and interfaces on the misfolding and subsequent aggregation of proteins are an important consideration in a number of biological and technologically important areas. For example the presence of an abundance of interfaces *in vivo* has resulted in a number of studies that were designed to assess the role played by model biological membranes and synthetic surfaces on the stability of proteins [1-4]. These separate studies showed that the presence of surfaces and interfaces can have a profound effect on aggregate development and that the growth rates and final aggregate morphologies are sensitive to the details of the surface chemistry of an interface (e.g. hydrophobicity, charge etc.). However, many of these studies are semi-quantitative in nature and a more quantitative measure of the effects of surfaces and interfaces on the stability of proteins remains to be obtained.

Interfacial effects are particularly important for a number of protein conformational disease related states that involve the aggregation of protein molecules into long fibrous structures called amyloid fibrils. These structures typically comprise linear aggregates of smaller protein units (e.g. monomers and dimers). They have diameters which are comparable to the dimensions of one or two protein molecules and can be many microns in length. These structures and their precursors have been linked to a number of diseases such as Alzheimer's disease, Huntingdon's disease, Parkinson's disease, Type II Diabetes and CJD [5-8]. In each case, the aggregates that are formed from different proteins have been found to exhibit very similar morphologies and to contain large amounts of chain folded intermolecular β-sheet structures. This has recently led to the conclusion that amyloid fibril formation is a generic property of proteins [5-8]. As a result, a significant amount of research has been carried out to try to develop an understanding of the molecular level processes that result in their formation. The fact that these structures are usually formed in the presence of a wide range of biological interfaces also suggests that developing a greater knowledge of how protein/surface interactions affect the formation of these structures could help us to understand these processes.

Recent developments in the rapidly emerging field of nanotechnology also raise some important questions about the effects of surfaces and interfaces on the stability and aggregation properties of proteins and other biological macromolecules [9]. Nanoscale materials and particles such as those being used in novel bio-sensing applications [10], immunological assays and early gene gun based delivery methods [11] have surface to volume ratios that are up to 10^8 times larger than bulk samples of the same materials. The surface related effects that have already been reported in studies of protein aggregation [1-3] therefore have important implications for the nanotoxicology of a wide range of materials.

Protein aggregation is also of considerable interest to the pharmaceutical industry, where maintaining the stability of proteins at low pH is vital during the production and purification of protein based drugs such as insulin [12-14]. The storage of proteins is also an important factor in determining the shelf life of these materials. In particular, the

effects of storing and processing proteins such as insulin in different containers are likely to affect their long term stability.

In this article we describe an experimental study of aggregation and amyloid fibril formation in bovine pancreatic insulin (BPI) at elevated temperatures and low pH. Fourier transform infrared (FTIR) spectroscopy and attenuated total reflection (ATR) spectroscopy are used to monitor the aggregation/β-sheet formation kinetics of this protein in bulk solution and on model hydrophobic polystyrene surfaces. The temperature dependence of the nucleation/lag times and aggregation rates associated with insulin fibril formation are used to determine the energy barriers associated with the nucleation and growth of these structures respectively. Complementary techniques such as atomic force microscopy (AFM), dynamic light scattering (DLS) and Thioflavin-T fluorescence assays were also used to monitor the growth of the protein aggregates. To the best of our knowledge, these experiments represent the first quantitative study of the effects of surfaces and interfaces on the aggregation properties of proteins.

EXPERIMENTAL

Stock solutions of 0.025M NaCl and 0.1M HCl (pH 1) were prepared in pre-boiled deuterium oxide (D_2O, Goss Scientific, Essex, UK). These solutions were then sealed in 15ml sample vials and degassed by placing them in a water bath at ~ 85^oC for 1 hour. The solutions were then allowed to cool to room temperature. BPI (Sigma Aldrich, Gillingham, UK, Mw=5733, cat. no. I5500) was then dissolved in the solutions at a concentration of 20$mgml^{-1}$ (~ 3.5mM). A single batch of BPI was used in all the experiments described below as batch-to-batch variations in the properties of insulin have been reported [15]. The resulting protein solutions were then left at room temperature in sealed vials for a further 24 hours to enable the complete hydrogen-deuterium exchange of labile hydrogens on the insulin molecules.

A. Fourier Transform Infra-Red Spectroscopy

FTIR Spectroscopy measurements were collected using a Varian FTS40 Pro spectrometer equipped with Resolutions Pro 4.0 software. Each averaged spectrum was collected using a spectral resolution of 4cm^{-1} and the time between the collection of the averaged spectra was 15 seconds. Deuterium oxide was used as the solvent in these experiments to avoid difficulties associated with the overlap of liquid water peaks with the Amide I and Amide II regions of the protein IR spectra. No spectral subtraction was performed on the infrared spectra. However, the baseline of the spectra tilted during the experiments due to variations in the intensity of the IR light source used in the spectrometer. This tilting was corrected for by subtracting a linear baseline which was calculated using the flat regions of the spectra in the ranges 850-1100cm^{-1} and 1750-2100cm^{-1}.

Bulk solution infrared (IR) spectroscopy measurements were performed over a range of temperatures from 60^oC to 80^oC using an electrically heated liquid transmission cell with Zinc Selenide (ZnSe) windows (Specac, Orpington, UK). One of the ZnSe windows was pre-drilled with two holes through its larger faces to allow the cell volume to be

exchanged with fluid. Prior to the experiments, one side of each ZnSe window was spin coated with a 2wt % solution of polystyrene (M_w = 600KDa, M_w/M_n = 1.09, Polymer Source) in toluene (spin speed 2500 rpm) and then annealed under vacuum at ~ 120^oC to remove residual solvent. This resulted in the formation of a ~ 200 nm thick polystyrene film (as measured using atomic force microscopy). This was done to protect the windows from the acidic solutions used in the experiments. Acidic solutions are known to dissolve ZnSe and Zn^{2+} ions have been shown to promote the onset of fibril formation in some proteins [16].

The two ZnSe windows were then placed together with their PS coated surfaces separated by a 75 μm thick poly (tetrafluoroethylene) (PTFE) spacer. This procedure was used to produce a small cavity with a 75 μm thick path length for performing liquid transmission IR studies. The resulting assembly was then sealed around the edge using a highly viscous solution of PS in toluene. The windows and spacer were then annealed at ~ 100^oC for 2 hours to remove residual toluene and to seal the edges of the cell so that it would not leak when filled. The window assembly was then placed in the sample cell and loaded into the sample chamber of the FTIR spectrometer. Stainless steel tubing was then attached to the sample cell so that the volume of the cell could be exchanged from outside the FTIR sample chamber. The chamber was then purged with dry air.

The fully assembled liquid cell was then heated to the desired experimental temperature which was monitored using a pre-calibrated t-type thermocouple buried in the metal body of the cell (close to the ZnSe windows). Deuterium oxide based stock solution was then injected into the cell. A background spectrum was collected by averaging 100 individual spectra and the stock solution was replaced with an identical solution containing 20$mgml^{-1}$ of BPI. Immediately after the injection of the protein solution, spectra were collected with a time resolution of 15 seconds. In each case 15 spectral scans were averaged per spectrum. All spectra were then ratioed to the spectrum obtained from the D_2O stock solution.

FTIR spectra of BPI adsorbed at PS surfaces were also collected using an ATR liquid cell (Specac). The ATR geometry uses the total internal reflection of IR radiation at a ZnSe/solution interface to produce an evanescent field that penetrates ~ 1μm in to the solution. As the intensity of this field decays exponentially as a function of distance, the IR spectra that are obtained using this technique are extremely sensitive to material that is close to the interface.

Thin films (~ 200nm) of PS were spin coated on to one side of a ZnSe ATR crystal using the same experimental parameters used to coat the ZnSe windows described above. The PS coated crystal was then annealed under vacuum at ~ 120^oC to remove residual solvent and then allowed to cool to room temperature. The ATR crystal was then loaded into the ATR liquid cell and heated to the required temperature using a circulating water bath. The temperature in the cell was monitored using a thermocouple embedded in the ATR cell top plate that had been pre-calibrated against the measured temperature inside the cell. The sample cell was then filled with the D_2O based stock solution and allowed to equilibrate before a background spectrum was collected by averaging 100 individual

spectra. The solution was then replaced with an identical solution containing $20 mgml^{-1}$ BPI and spectra were collected every 15 seconds (averaging 15 scans per spectrum).

B. Atomic Force Microscopy of BPI aggregates

BPI was dissolved in the D_2O based stock solutions at a concentration of $20 mgml^{-1}$. Bulk solution insulin fibrils were formed by incubating sealed vials of the resulting protein solution in a water bath at 60 ^oC. The vials were then removed at regular time intervals and placed in an ice bucket to slow down the fibril growth rates and quench in the structure of the fibrils.

Surface adsorbed fibrils were prepared on PS coated single crystal silicon wafers (Si, Compart Technology, [100], ~ 300 μm thick). A ~ 200nm thick PS film was spin coated on to the Si wafers from a 2wt% solution in toluene and annealed at 120 ^oC under vacuum. The resulting PS films were then submerged (facing downwards) in vials containing similar solutions to those used to form the bulk fibrils and were incubated in a water bath at 60 ^oC. The sealed vials were then removed at regular time intervals and quenched in a bucket of ice.

In the case of the bulk solution fibrils, a droplet of each protein solution was transferred on to a clean PS coated Si wafer and allowed to dry before being imaged with an Asylum Research MFP-3D AFM. The fibrils formed on the PS surfaces were simply allowed to dry out before being imaged. All samples were imaged using tapping mode AFM.

B. Dynamic light scattering studies
C.

The time evolution of the average aggregate size in $20 mgml^{-1}$ solutions of BPI in D_2O based stock solutions were studied at a temperature of 60^oC using a Malvern Instruments DLS (4700 PCS).

D. Thioflavin-T studies

Thioflavin-T (ThT) fluorescence studies were used to monitor the kinetics of β-sheet formation during aggregation/fibril formation in BPI. Solutions of BPI ($20 mgml^{-1}$) containing ~ 2.5 μM ThT were placed on a glass cover slip inside a ~ 10mm diameter o-ring. A second cover slip was then clamped on top of the o-ring to create a sealed sample cell. The cell was then placed on top of a home made heater and mounted on the stage of an Olympus BX51 optical microscope equipped with fluorescence capabilities, a DP70 CCD camera and connected to a PC running Image Pro Plus software (Media Cybernetics). The protein solution was then heated to 60 ^oC and the excited fluorescence measured through a filter ($\lambda \sim$ 470-490 nm, U-MNB2, Olympus) using the CCD camera. Optical micrographs of the solution in the sample cell were then collected at 30 second intervals. The Image Pro Plus software was then used to determine the average fluorescence intensity obtained from the optical micrographs as a function of time.

RESULTS AND DISCUSSION

Figure 1 shows an example of a typical FTIR spectrum of the amide I and II regions that was obtained using the bulk liquid transmission cell. Spectra obtained from both the bulk liquid transmission cell and the ATR cell had similar features. Minor differences in the spectra were attributed to the wave-number dependence of the penetration depth of the evanescent field in the ATR experiments. The spectra obtained for the combined amide I and II regions were fitted to five Lorentzian peaks (shown as the grey lines in figure 1) using a non linear least squares fitting algorithm. The assignments of these peaks are given in the inset of figure 1. The sum of all these peaks is shown as the black solid line in the main panel of figure 1. The assignments of the peaks in the amide I region are consistent with literature reports of the positions of peaks that correspond to features associated with β-sheet, random coil and α-helix [17-19]. The two peaks used to represent the amide II region in our fitting procedure do not have any specific assignments and were simply used to describe the shape of the spectra. The shape of this region did not change during the course of the FTIR experiments and these peaks were found to represent the shape of the amide II region accurately (see figure 1).

The fitting procedure was performed on all the spectra collected from each FTIR experiment. The positions of all but the β-sheet peak (1610-1633cm^{-1}) were constrained to within ± 2cm^{-1} and the widths were constrained to within ± 5 cm^{-1}. The position of the β-sheet peak was allowed to vary by ±12 cm^{-1} as reports by Nielsen and coworkers suggest that the position of this peak changes during the aggregation of insulin [17]. The amplitudes of all the peaks were not constrained and were allowed to vary during the fitting procedure.

For each set of data, the last spectrum to be collected was fitted first. The spectrum collected immediately before this was then fitted using the parameters (positions, widths and amplitudes of all the peaks) obtained from the previous spectrum as the new initial guess for the fit parameters. This process of working backwards through the spectra was repeated for all the spectra collected in a single experiment. The fitting procedure typically gave an initial value for the ratio of the areas of the fitted peaks of 7% / 54% / 39% (β-sheet/α-helix/random coil). The final value of this ratio was typically found to be 76% / 20% / 4%. These values are in agreement with results obtained from other studies of insulin aggregation [17, 19, 20].

The areas of the peaks obtained from the fitting procedure were then used to generate plots of the kinetics of β-sheet growth, similar to those shown in figure 2. To decouple the effects of changes in the β-sheet content of the BPI molecules from effects due to changing amounts of protein in the beam path, the area of the β-sheet peak was divided by the sum of the areas of the two peaks used to fit the amide II region of the FTIR spectra (see figure 1). The shape of the amide II peak did not change during the experiments indicating that this peak was insensitive to structural changes in the BPI molecules. This result is consistent with the results obtained by Hiramatsu and coworkers [21]. The amide II peak was therefore used as a measure of the amount of protein in the beam path. Dividing the area of the β-sheet peak by the area of the amide II region in this

way therefore gives a measure of the extent of β-sheet formation per unit mass of protein during aggregation/fibril formation.

As shown in the inset of figure 2, the total area of the amide II peak increases with time during the ATR experiments on PS surfaces. This increase was attributed to changes in the amount of insulin at the PS/water interface caused by the continued adsorption and aggregation of insulin at the PS surfaces. The area of the amide II peak measured in the bulk transmission cell experiments did not change appreciably during the course of the experiments. This is to be expected because the amount of protein in the IR beam path remains constant during these experiments.

Figure 2 shows that the β-sheet kinetics curves obtained from the bulk transmission and ATR experiments are similar but not identical. In each case, the β-sheet content of the protein aggregates was found to display two stage kinetics. The initial phase of β-sheet growth rapidly saturated after ~ 400 - 700 seconds and was found to exhibit only a weak temperature dependence. This initial growth stage in the kinetics was also found to occur on similar timescales in both the ATR and bulk transmission studies.

DLS and ThT fluorescence studies performed at $60^{o}C$ revealed that this first stage in the β-sheet kinetics was produced by the rapid formation of protein aggregates with an average radius of 13 ± 1 *nm* (see figure 3). The correspondence between the features observed in the FTIR data, the dynamic light scattering experiments and the ThT fluorescence measurements indicate that these initial aggregates contain significant amounts of intermolecular β-sheet (see figures 2 and 3). The presence of a measurable ThT intensity (above background levels) in the plateau region also suggests that repeat β-sheet folds are present in these aggregates [22]. However, AFM images of the samples did not show the presence of any fibrils (or fibril precursors) in the bulk solution or on the PS surfaces during this initial period of β-sheet growth (see inset figure 2). Only small, less well defined aggregates were observed with the AFM in this time period. The presence of nanoscale non-fibrillar aggregates have also been reported for other small polypeptides [23] during studies of fibril formation. We note at this point that great care must be taken when interpreting the AFM images shown in figure 2. The drying of protein solutions is often unreliable and can lead to different quantities of fibrils and other aggregates being observed on what should be identical samples. However, if sufficient AFM images are collected, this technique can be used to confirm the presence or absence of fibrils and to make qualitative comparisons between the morphologies of the aggregates that are formed.

A key point about the smaller aggregates formed in the initial stages of the present study is that they appear to form independently of the fibrils and do not have a significant influence upon fibril nucleation and growth. This was deduced from that fact that the formation of these structures showed much weaker temperature dependence than the nucleation/lag times associated with fibril formation. If the formation of fibrillar nuclei was influenced by the presence of these smaller aggregates then we would expect to observe a correspondence between the temperature dependence of the fibril nucleation rates and the rates associated with the formation of these smaller aggregates.

The second, more rapid region of β-sheet formation was attributed to the growth of fibrils and was mirrored in both the ThT fluorescence and dynamic light scattering studies. The presence of fibrils was confirmed by collecting AFM images of both PS surface adsorbed and bulk solution protein (see inset fig. 2). The onset of fibril formation was found to occur earlier at PS/water interfaces than in bulk solution and the initial rates of fibril growth/β-sheet formation were found to be slower on the PS surfaces (as determined from the slopes of the curves in the main panel of fig. 2). Qualitatively this indicates that fibril nucleus formation occurs faster on the PS surfaces than in bulk solution. The reduction in the growth rates associated with the β-sheet formation kinetics on the PS surfaces also indicates that the presence of the PS surface hinders the growth of insulin fibrils.

A consideration of the kinetics of the changes in the area of the amide II peak for the PS surface experiments (see inset in figure 2) indicates that the amount of protein at the interface did not increase significantly until the onset of fibril growth. At this point, the amide II peak area increases along with the area of the inter-molecular β-sheet peak. This is likely to be due to a combination of effects related to the addition of protein molecules to surface nucleated fibrils (elongation) and the adsorption of bulk nucleated fibrils on the PS surfaces (deposition).

The final saturation point in the β-sheet absorbance kinetics were found to be similar for the PS surface and bulk solution at each temperature studied. At the point where the β-sheet kinetics saturated, the BPI solutions were found to form a viscous opaque gel. Cryo-Scanning electron microscopy of these gels revealed that they contain a large tangled network of mature fibrils (data not shown).

In the bulk solution IR studies, the absorbance changes ($A(t)$) measured in the second stage of the β-sheet growth kinetics were found to follow an exponential rise of the form

$$A(t) = A_p + \left(A_o - A_p\right)\left(1 - \exp\left(-\frac{t-\tau_n}{\tau_a}\right)\right) \quad (1)$$

where A_p and A_o are the absorbance values in the first plateau region and at saturation respectively. The quantities τ_n and $1/\tau_a$ represent the fibril nucleation/lag time and growth rate respectively.

Figure 4 shows semi-logarithmic plots of the reduced absorbance ($1 - A(t)/A_o$) versus time for bulk solution protein (panel a) and PS surface adsorbed protein (panel b) at a range of temperatures between 60 ^oC and 80 ^oC. According to equation 1, a plot of $\log_e (1 - A(t)/A_o)$ vs. time should produce a straight line in the region corresponding to fibril growth with a slope that is equal to the aggregation rate, $1/\tau_a$. As can be seen in the top panel of figure 4, this region in the bulk data is accurately fitted by a single straight line. In the case of the PS adsorbed protein, two such linear regions exist (figure 4, bottom panel). The first slope is shallower than the slope observed for the bulk solution studies and occurs at earlier times. This slope was attributed to the formation of fibrils by insulin

molecules that interact directly with the PS surface. AFM images of the PS surfaces taken during the period corresponding to the initial slope in the second stage of β-sheet growth showed evidence of a number of BPI fibrils (see inset, figure 2). The second slope in the PS surface data started at similar times and had comparable (but not identical) slopes to those observed in the bulk solution studies. This region was attributed to the bulk component of the signal acquired in the ATR experiments performed on the PS surfaces. These data are expected to show some features of the bulk solution response of the protein because the evanescent field used to probe the PS/water interface extends ~ $1\mu m$ into the solution. Although ATR is predominantly surface sensitive, the penetration depth of the evanescent field will extend beyond the thickness of any adsorbed protein layers and as a result, will be sensitive to insulin molecules in bulk solution.

In each case, the slope of the linear regions was used to determine the aggregation/β-sheet growth rates ($1/\tau_a$) associated with the formation of BPI fibrils. The natural logarithm of the aggregation rate was then plotted against the inverse of temperature to produce Arrhenius plots for both bulk solution data and the PS surface data (see top panel, figure 5). The PS surface data shown in figure 5 is split into two components. The first corresponds to the bulk component of the aggregation measured in the ATR experiments and the second corresponds to the true PS surface component of the data. This figure shows that the aggregation rates obtained from figure 4 are faster in bulk solution than on the PS surface. Moreover, the bulk solution aggregation rates appear to be faster than the bulk component of the aggregation kinetics measured using the ATR cell. This is discussed in more detail below.

The linear fits to the aggregation rate data shown in figure 5 were used to determine the energy barriers associated with fibril formation according to the Arrhenius equation

$$\log_e\left(\frac{1}{\tau_a}\right) = \log_e\left(\frac{1}{\tau_{a,o}}\right) - \frac{E_a}{RT} \quad (2)$$

where E_a is the energy barrier associated with fibril formation ($Jmol^{-1}$), R is the molar gas constant ($Jmol^{-1}K^{-1}$), T is the temperature (K) and $1/\tau_{a,o}$ is a characteristic attempt frequency associated with fibril growth (s^{-1}). At this point we note that the values of $1/\tau_a$ shown in figure 5 represent an average measure of the growth rates of all the aggregates in the system and not the individual fibril elongation rates. However, the amount of β-sheet formed in the system is expected to be directly proportional to the length of the fibrils formed. This means that under a given set of solution conditions, the aggregation/β-sheet formation rates shown in this figure will be related to the average fibril elongation rate by a simple numerical factor. However, the fact that E_a is derived from the temperature dependence of these scaled aggregation rates means that E_a represents a measure of the true energy barrier for fibril growth.

The values obtained for the energy barrier, E_a from figure 5 are summarised in table 1. The values shown are comparable to values that have been reported for proteins/peptides of comparable size and under similar solution conditions [23]. Table 1 clearly shows that the energy barrier associated with the growth of fibrils on PS surfaces is larger than the

corresponding barrier associated with bulk solution fibril growth, within the limits of experimental uncertainty. This suggests that it is more difficult for fibrils to grow on hydrophobic PS surfaces than in bulk solution. The reason for this could be interpreted in a number of ways. The energy barriers presented in table 1 represent a composite barrier which describes the change from the native solution state of the protein to an aggregated state. This energy barrier is therefore likely to include separate energy contributions due to differences in protein concentration and the colloidal and conformational stability of the protein molecules [15]. The concentration and conformation of protein molecules adsorbed at the hydrophobic polymer surface and at the end of adsorbed fibrils are likely to differ from similar molecules in solution. These factors would be expected to alter the collision probabilities and folding pathways associated with the attachment of protein molecules to the end of the growing fibril and would influence the corresponding contributions to the measured free energy barrier. The presence of charged protein molecules close to a dielectric material such as polystyrene could also induce polarisation charges in the polymer films which would alter the charge distribution around the tip of an adsorbed growing fibril. All of these factors could contribute to the observed differences in the aggregate/fibril growth barrier, but they are difficult to quantify in the context of the present study.

It is also noteworthy that the energy barrier derived from the bulk component of the aggregation measured in the ATR experiments is larger than the energy barrier determined from bulk solution IR transmission measurements. As shown in figure 5 and table 1, the aggregation rates and the energy barrier determined from the bulk component of the PS surface data fall in between those obtained for the 'true' measured bulk and surface values. To determine the cause of this apparent discrepancy, a simple experiment was performed where BPI was absorbed at a PS surface and the excess bulk solution protein was then flushed from the cell using the D_2O based stock solutions. Measurement of the ATR spectra before and after flushing the cell showed that the measured absorbance due to surface adsorbed protein represented ~ 50% of the total measured signal. This accounts for the fact that the energy barrier and aggregation rates for the bulk component of the PS surface data appear to be weighted averages of the corresponding bulk and surface values.

In addition to being used to determine the aggregation rates, the plots shown in figure 4 were also used to estimate the characteristic *nucleation* or *lag* times, τ_n, for the onset of fibril growth. This was done by determining the point of intersection of the fibril growth rate fit lines with the horizontal dashed lines used to define the plateau region in the kinetics (see figure 4). These nucleation times were then used to define an effective *nucleation rate,* $1/\tau_n$. The resulting nucleation rates are plotted on an Arrhenius diagram in the bottom panel of figure 5. The plots shown in figure 5 were used to extract the energy barriers (E_n) and attempt frequencies $1/\tau_{n,o}$ associated with the onset of fibril formation, using a similar procedure to that described for the fibril growth rates. The values of (E_n) that were obtained for the bulk solution and PS surface studies are summarised in table 1. The energy barriers to fibril nucleation shown in table 1 are comparable to (but smaller than) those observed for the aggregation of peptide chains of a similar size [24]. As shown in table 1, the nucleation barriers in all three cases are the

same within the limits of experimental uncertainty. Initially, this may seem counter intuitive given that there are clear observable differences in the measured nucleation rates for the bulk and PS surface data sets (see figures 4 and 5). The presence of a hydrophobic interface might also be expected to cause the protein to unfold to expose more hydrophobic residues in the core of the insulin molecules to the PS surface. This would be expected to result in both a decrease in the enthalpy of interaction and an increase in the conformational entropy of the protein molecules [1] adsorbed at the PS/water interface. These combined factors would act to reduce the free energy barrier associated with the unfolding and subsequent aggregation of the protein. However, it is worth considering that the conformations adopted by the insulin molecules at the PS surfaces would not necessarily correspond to viable fibril forming intermediate states. As a result, a surface unfolded insulin molecule could experience a local conformational free energy barrier that is similar to that of a protein in bulk solution. The energy barrier associated with fibril nucleus formation would therefore not necessarily be altered significantly by forcing the protein to unfold at an interface.

In spite of the fact that the fibril nucleation barriers are not significantly changed, figure 5 shows that the rates associated with the formation of fibril nuclei are increased by the presence of the PS surface. If the energy barriers associated with fibril nucleus formation remain unchanged, this suggests that the characteristic attempt frequencies associated with nucleus formation must be larger (see equation 2). One possible reason for this could be related to differences in the concentration of protein molecules in the bulk and on the PS surfaces. In the ATR experiments, the PS surfaces were rapidly coated (within 15 seconds) with a surface excess of insulin. This resulted in a larger local protein concentration at the surface than in bulk solution. The localisation of a 'dense' layer of protein at the PS surface would therefore increase the probability of two insulin molecules coming into contact and would result in a corresponding increase in the attempt frequency associated with the formation of viable fibril nuclei.

Regardless of the mechanism that is responsible for the accelerated formation of fibril nuclei, this experimental observation has some potentially far reaching implications with regards to the toxicology of high surface area nanoscale materials. Fibril precursors have recently been implicated as being the toxic species in a number of amyloid related diseases [25]. As these experiments show, the presence of artificial surfaces such as the model PS surfaces studied causes the more rapid formation of these fibril precursors or nuclei. This means that great care must be taken to assess the full toxicological impact of new nanoscale diagnostic and therapeutic agents before they are released on to the market.

The time scales associated with both the nucleation and growth of fibrils shown in figure 4 are similar to those reported for insulin under similar solution conditions [26]. At the temperatures studied, the fibril nucleation and growth rates (see figure 5) have values that vary between $\sim 1 \times 10^{-4}\ s^{-1}$ and $\sim 2 \times 10^{-2}\ s^{-1}$. The characteristic time associated with the folding of a β-sheet 'hair pin' structure has been reported for peptide chains that are comparable in size to an insulin molecule [23, 27]. These studies showed that the time associated with the folding of a β hairpin structure for an isolated peptide chain is of the

order of ~ 20 μs, but that the timescales associated with formation of intermolecular β-sheet structures during aggregation can be significantly longer (~ 2ms). These time scales correspond to rates of ~5 × 10^4 s^{-1} and ~ 500 s^{-1} respectively. The aggregation/fibril growth rates measured in the present study are up to 10^8 times smaller than the rates associated with the formation of intermolecular β-sheet. This suggests that conformational changes alone are not sufficient to account for the aggregation rates measured here and that the growth rates of insulin fibrils at the pH and salt concentrations studied are also mediated by other factors such as colloidal stability [15]. This is not surprising when consideration is given to the fact that the isoelectric point of insulin occurs at 5.3 [28] and the pI of the solutions studied is 1. Under such solution conditions, each insulin molecule would be expected to carry a net charge of ~9.6 × 10^{-19} C (+6e) [1, 17]. This would result in the formation of charged double layers [29] around the insulin molecules that would repel neighbouring proteins and reduce the associated aggregation rates.

In each case the characteristic attempt frequency ($1/\tau_o$) was typically found to lie in the range 10^{12} - 10^{14} s^{-1}. This is comparable to the high temperature relaxation rate of a simple liquid (~ 10^{13} s^{-1}) and represents a reasonable upper bound for the attempt frequency [23]. This is because both fibril nucleation and growth are expected to involve the translation of molecules from the surrounding solution environment to the tip of the growing fibril. However, a more detailed analysis of the attempt frequencies would be unrealistic as these values are obtained by extrapolating the aggregate growth rates by over ten orders of magnitude.

CONCLUSIONS

A new method has been presented for determining the rates of aggregation and the energy barriers associated with insulin fibril nucleation and growth in bulk solution and at model PS surfaces. These experiments showed that the presence of hydrophobic PS surfaces promoted the nucleation of fibrils but did not affect the size of the fibril nucleation barrier (within error). The PS interface did however increase the energy barrier associated with the growth/elongation of insulin fibrils. These observations were briefly explained in terms of the differences in conformational and colloidal stability of the proteins in solution and on surfaces, as well as differences associated with protein concentration effects and the mobility of the insulin molecules. The method described in this work involves the use of well established IR spectroscopy based protein characterisation methods and we anticipate that this technique could also be used to study aggregation in other protein/surface systems.

Acknowledgments

We thank Dr Sno Stolnick (School of Pharmacy) for providing access to the dynamic light scattering apparatus. We are grateful to the University of Nottingham's Interdisciplinary Doctoral Training Centre (IDTC) in Nanotechnology for providing access to a project studentship for this work. We also thank the Engineering and Physical

Sciences Research Council, the Nuffield Foundation and the University of Nottingham for providing funding.

References

[1] J.S. Sharp, J.A. Forrest and R.A.L Jones, *Biochemistry*, 41, 15810-15819, (2002)
[2] S. Adams, A.M. Higgins and R.A.L. Jones, *Langmuir*, 18, 4854-4861, (2002)
[3] M. Zhu, P.O. Souillac, C. Ionescu-Zanetti, S.A. Carter and A.L. Fink, *J. Biol. Chem.*, 277, 50914-50922, (2002)
[4] V. Sluzky, J.A. Tamada, A.M. Klibanov and R. Langer, *PNAS*, 88, 9377-9381, (1991)
[5] C.M. Dobson, *Nature*, 426, 884-890, (2003)
[6] A. Ahmad, I.S. Millet, S. Doniach, V.N. Uversky and A.L. Fink, *Biochemistry*, 42, 11404-11416, (2003)
[7] A.K. Chamberlain, C.E. MacPhee, J. Zurdo, L.A. Morozova-Roche, H. Allen, O. Hill, C.M. Dobson and J.J. Davis, *Biophysics*, 79, 3282-3293, (2000)
[8] E. Žerovnik, *Eur. J. Biochem.*, 269, 3362-3371, (2002)
[9] *Nanoscience and nanotechnologies: opportunites and uncertainties, The Royal Society & The Royal Academy of Engineering, UK*, (2004)
[10] A. Vaseashta and D. Dimova-Malinovska, *Sci. Tech. Adv. Mat.*, 6, 312-318, (2005)
[11] B.K. Tischer *et al., J. General Virology*, 83, 2367-2376, (2002)
[12] E.Y. Chi, S. Krishnan, T.W. Randolph and J.F. Carpenter, *Pharm. Res.*, 20, 1325-1336 (2003)
[13] , L.N. Garriques, S. Frokjaer, J.F. Carpenter and J. Brange, *J. Pharm. Sci.*, 91, 2473-2480 (2002)
[14] A. Ahmad, V.N. Uversky, D. Hong and A.L. Fink, *J. Biol. Chem.*, 280, 42669-42675, (2005)
[15] J. Brange, L. Andersen, E.D. Laursen, G. Meyn and E. Rasmussen, *J. Pharm. Sci.*, 86 (5), 517-525, (1997)
[16] B. Raman, T. Ban, K. Yamaguchi, M. Sakai, T. Kawai, H. Naiki and Y. Goto, *J. Biol. Chem.*, 280, 16157-16162, (2005)
[17] L. Nielsen, S. Frokjaer, J.F. Carpenter and J. Brange, *J. Pharm. Sci.*, 90, 29-37, (2001)
[18] J.L. Jiménez, E.J. Nettleton, M. Bouchard, C.V. Robinson, C.M. Dobson and H. Saibil, *Proc. Nat. Acad. Sci.*, 99, 9196- 9201, (2002)
[19] M. Bouchard, J. Zurdo, E.J. Nettleton, C.M. Dobson and C.V. Robinson, *Protein Science*, 9, 1960-1967, (2000)
[20] M.R.H. Krebs *et. al, Proc. Nat. Acad. Sci. US*, 101(40), 14420-14424, (2004)
[21] H. Hiramatsu and T. Kitagawa, *Biochimica et Biophysica Acta*, 1753, 100-107, (2005)
[22] M.R.H Krebs, E.H.C Bromley and A.M. Donald, *J. Struct. Biology*, 149, 30-37, (2005)
[23] Y. Kusumoto, A. Lomakin, D.B. Teplow and G.B. Benedek, *Proc. Nat. Acad, Sci. US*, 95, 12277-12282, (1998)
[24] R. Sabaté, M. Gallardo and J. Estelrich, *Int. J. Bio. Macromol.*, 35, 9-13, (2005)
[25] R. Kayed *et al, Science* , 300, 486-489, (2006)
[26] M.R.H. Krebs, E.H.C. Bromley, S.S. Rogers and A.M. Donald, *Biophys. J.*, 88, 2013-2021, (2005)

[27] V.Muñoz, R. Ghirlando, F.J. Blanco, G. S. Jas, J. Hofrichter and W.A. Eaton, *Biochemistry*, 45, 7023-7035, (2006)
[28] A. Conway-Jacobs and L.M. Lewin, *Anal. Biochem.*, 43, 394-400, (1971)
[29] J. Israelachvili, *Intermolecular and Surface Forces, 2nd Ed.*, Academic Press, Oxford, (1991)

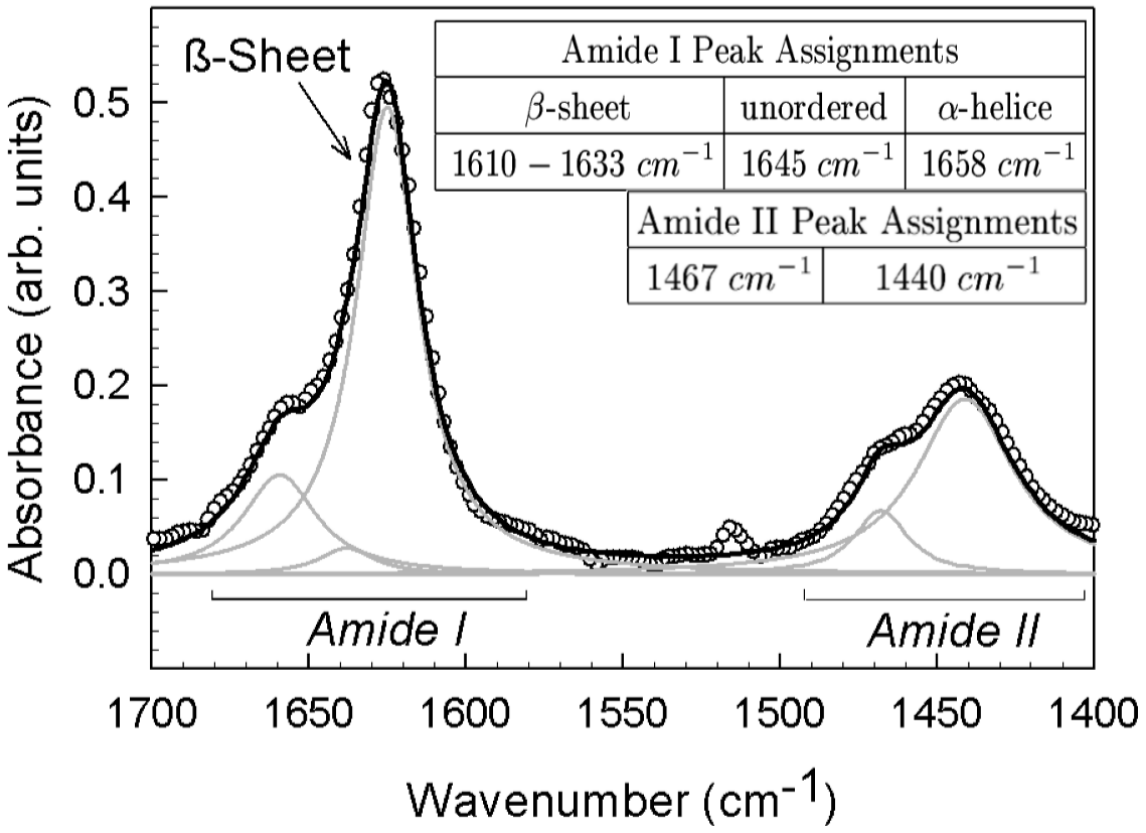

FIG. 1: Infrared spectrum of the Amide I and II spectral regions for bovine pancreatic insulin collected at $60^{o}C$ and pH 1 after being incubated for ~ 100 *mins*. The grey lines show the five Lorentzian peaks that were used to fit the data (○). The inset shows a table of the peaks used to fit the data along with their protein structural assignments [17]. The black solid line is the combined fit to the data and is given by summing the contributions of the five separate Lorentzian peaks.

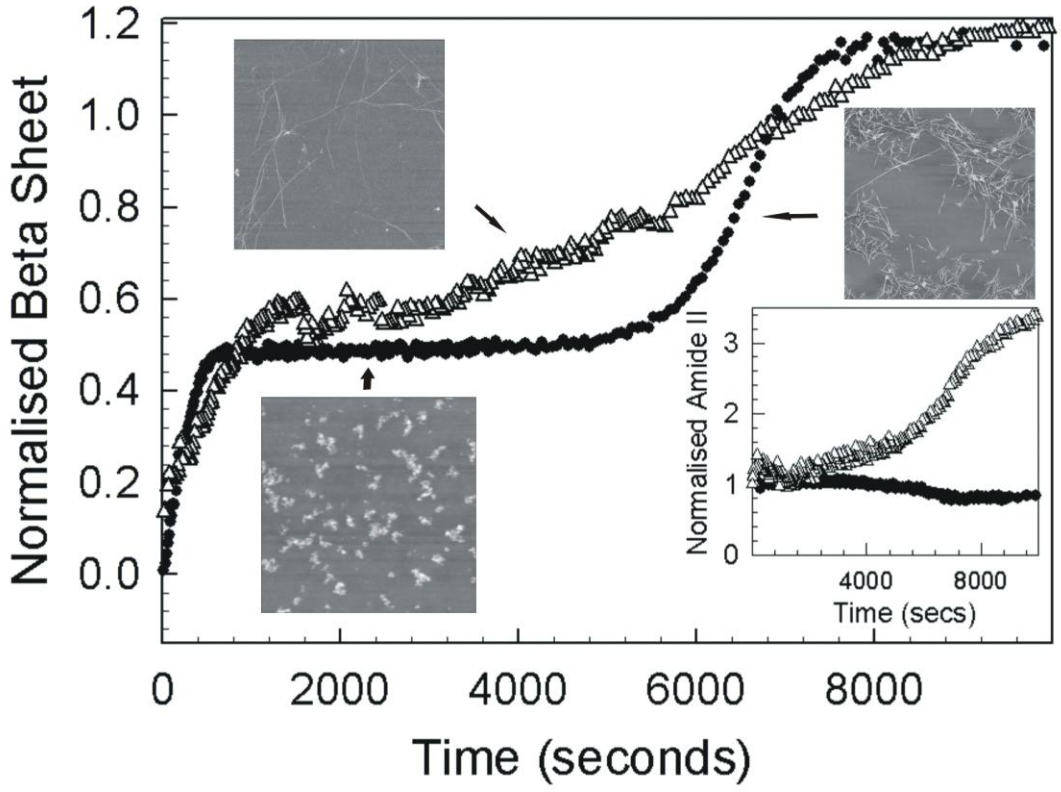

FIG. 2: Kinetics of β-sheet formation during the aggregation of bovine pancreatic insulin. Data are shown for insulin aggregating in bulk solution (●) and near a polystyrene surface (Δ). In both cases the area of the β-sheet peak was divided by the total area of the amide II region collected at each time. The inset shows a plot of the variation in the area of the amide II region with time. In both cases, the area of this peak was divided by the initial area of this region. All data were collected at a temperature of $60^{o}C$ and at pH 1. The AFM images shown as insets were collected using a scan area of 5 μm × 5 μm and show typical images of the observed aggregate morphologies at the times indicated by the solid arrows.

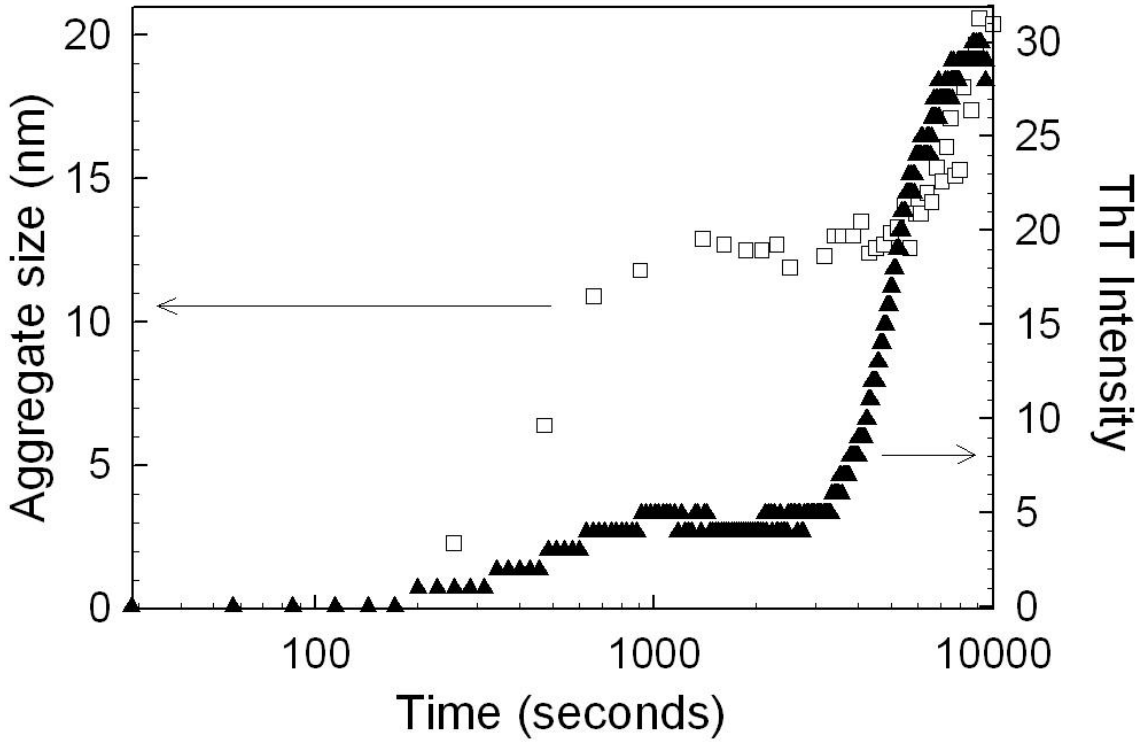

FIG. 3: Dynamic light scattering (□, left axis) and ThT fluorescence studies (▲, right axis) of the aggregation on bovine pancreatic insulin. All data were collected at a temperature of $60^{o}C$ and at pH 1.

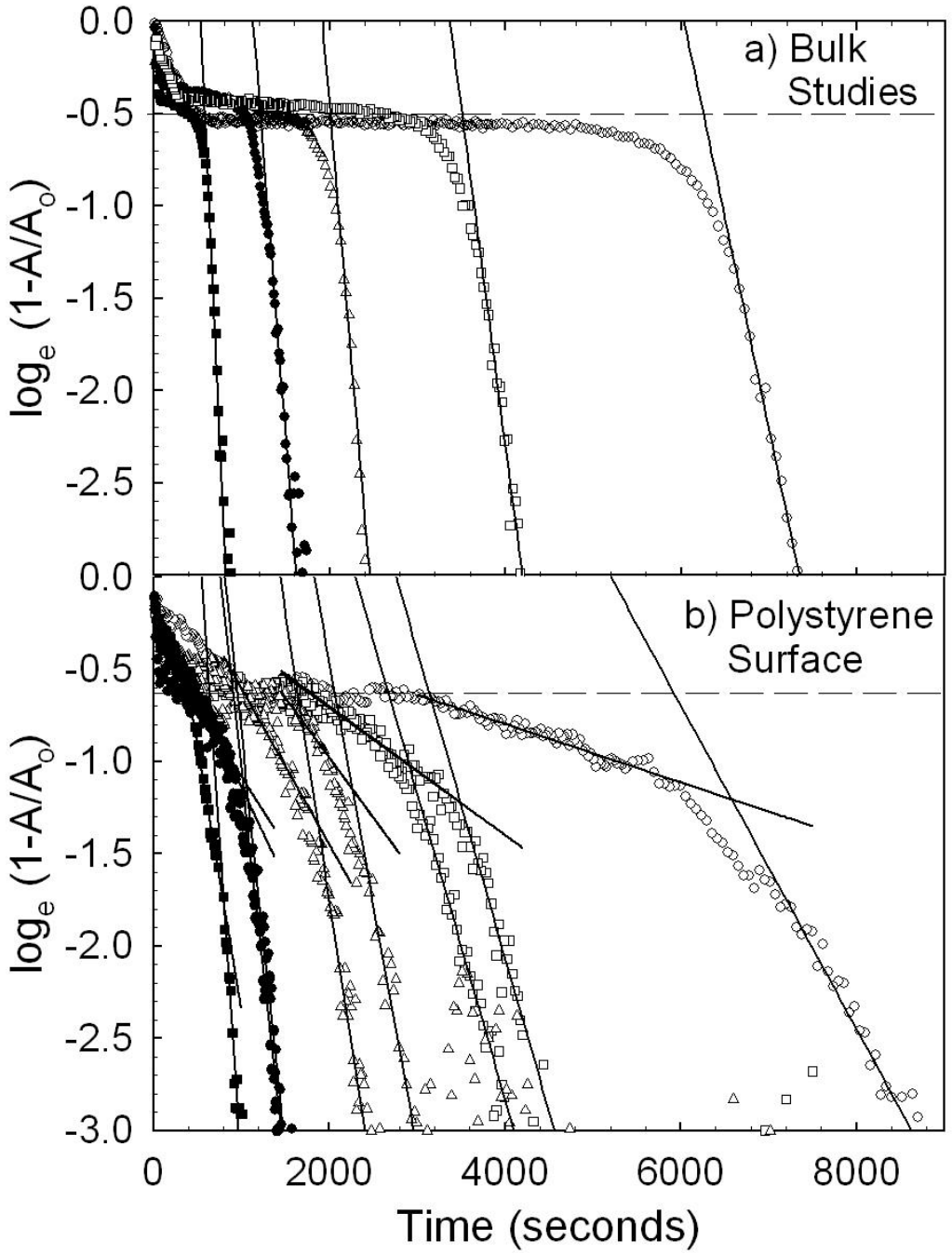

FIG. 4: Semi-logarithmic plots of the reduced β-sheet absorbance (1 - $A(t)/A_o$) of bovine pancreatic insulin versus time. Data are shown for the bulk aggregation kinetics (top panel) and for aggregation at a polystyrene surface (bottom panel). In both cases data were collected at pH 1 and at temperatures close to 60 ^oC (○), 65 ^oC (□), 70 ^oC (Δ), 75 ^oC (●) and 80 ^oC (■) respectively. All temperature values were measured with an uncertainty of ±1 ^oC. The solid black lines show the fits used to determine the aggregation rates (see text). The horizontal dashed lines mark the position of the plateau region ($A = A_p$) that was used in determining the nucleation / lag time for fibril formation (see text).

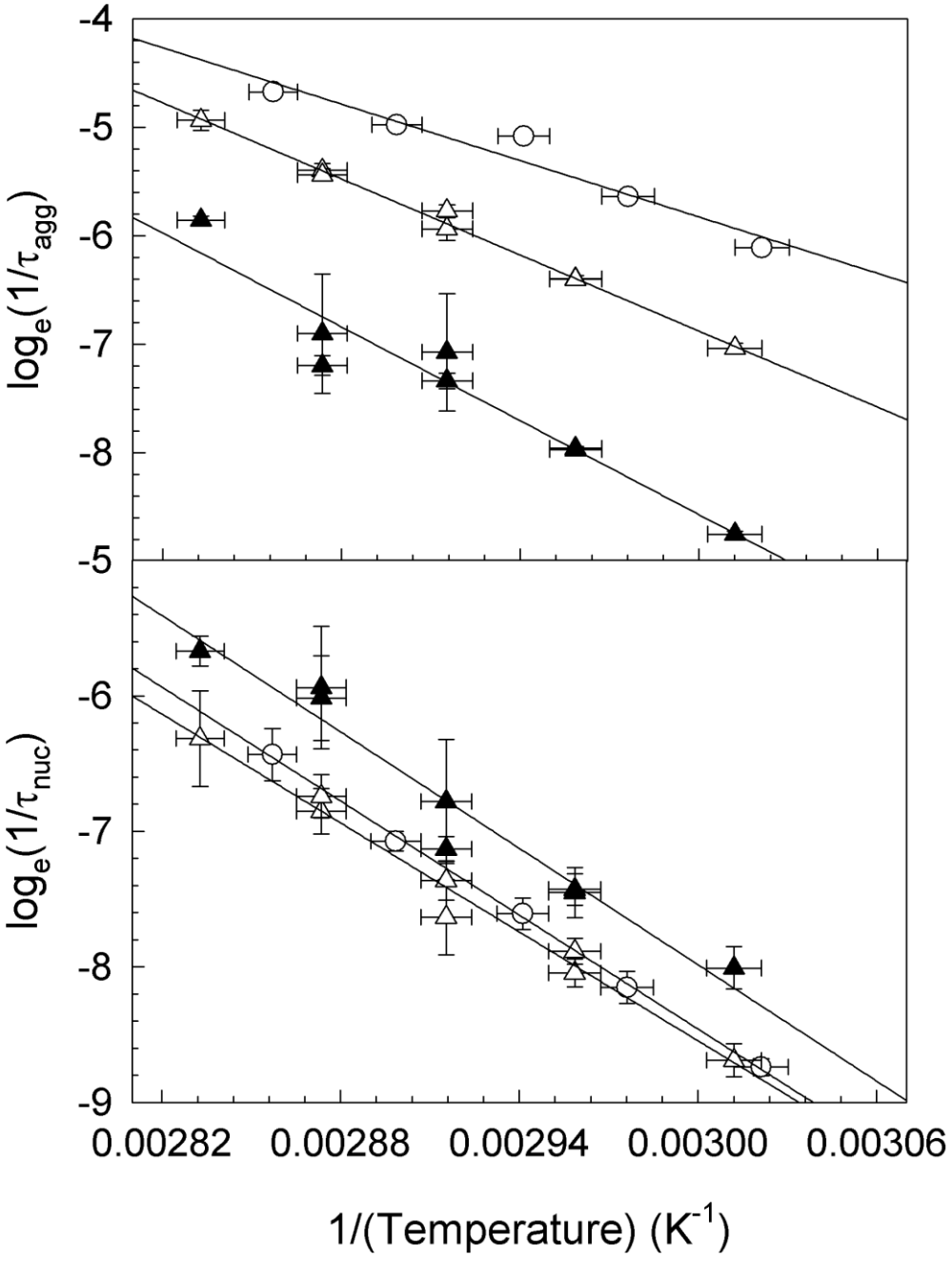

FIG. 5: Arrhenius plots of the aggregation/fibrillisation rates (top panel) and effective nucleation rates (bottom panel) of BPI at pH 1. Data are shown for bulk solution (○), the polystyrene surface data (▲) and the bulk component of the polystyrene surface data (Δ, see text). The solid lines represent fits to the form of equation 2.

Energy Barrier (KJ mol^{-1})	Nucleation	Fibril Growth
Bulk	117 ± 2	72 ± 10
Polystyrene (Bulk component)	111 ± 6	97 ± 3
Polystyrene (Surface component)	119 ± 11	120 ± 14

TABLE I: Energy barriers for fibril nucleation and growth